IEEE Access
Multidisciplinary | Rapid Review | Open Access Journal

Received November 16, 2019, accepted December 4, 2019, date of publication December 6, 2019,
date of current version December 23, 2019.

Digital Object Identifier 10.1109/ACCESS.2019.2958257

IoT-Linked Integrated NFC and Dual Band UHF/2.45 GHz RFID Reader Antenna Scheme

ADISAK ROMPUTTAL[1] AND CHUWONG PHONGCHAROENPANICH[2], (Member, IEEE)
[1]Department of Physics, Faculty of Science and Technology, Thammasat University, Pathumthani 12121, Thailand
[2]Department of Telecommunications Engineering, Faculty of Engineering, King Mongkut's Institute of Technology Ladkrabang, Bangkok 10520, Thailand

Corresponding author: Adisak Romputtal (radisak@tu.ac.th)

This work was supported by Thammasat University Research Fund under the TU Innovative Scholar, under Contract 6/2561.

ABSTRACT This research proposes a system board of integrated antenna scheme of near-field communication (NFC) and dual band ultra-high frequency (UHF, 920-925 MHz)/2.45 GHz radio frequency identification (RFID) reader antennas for Internet of Things (IoT) applications. The integrated antenna scheme is capable of simultaneous execution of NFC and UHF RFID functions whereby the NFC and UHF RFID modules, which are serially connected to a microcontroller with Wi-Fi module (NodeMCU), read the universal identification (UID) of NFC and UHF RFID tags. The data are then forwarded to a cloud server via Internet of Things (IoT) and are viewable on smartphones using Blynk mobile application via IoT. To realize the optimal antenna design, simulations were carried out using CST Studio Suite. Prototype antennas were subsequently fabricated and integrated into the system board for IoT-linked near- and far-field communication. The simulation and measured results are in good agreement. The NFC reader antenna resonates at 13.56 MHz, and the dual band UHF/2.45 GHz RFID reader antenna achieves the 920-925 MHz and microwave (MW) bands with high isolation. The novelty of the proposed integrated NFC and UHF RFID antenna scheme lies in the use of cloud technology to store real-time and archival data, in place of traditional servers. The integrated antenna scheme could achieve the NFC, UHF, and MW frequency bands, rendering it ideal for IoT applications.

INDEX TERMS Near field communication (NFC), radio frequency identification (RFID), NFC antenna, ultra-high frequency (UHF) reader antenna, dual band antenna, Internet of Things (IoT).

I. INTRODUCTION

Near field communication (NFC) is a short-range RFID-based wireless communication technology for data exchange via contactless data transmission at 13.56 MHz. Unlike RFID, NFC combines both contactless identification and interconnection technologies. NFC technology is thus widely adopted for contactless payment, access control, and diverse applications between electronic devices and smartphones.

Ultra-high frequency (UHF) and 2.45 GHz RFID technologies have been deployed in a multitude of applications because of their long-read range and high data transmission rates. To enjoy the best of both worlds, NFC and UHF/2.45 GHz RFID technologies could be integrated in response to growth in new applications in the area of Internet of Things (IoT).

In [1], the authors proposed a circularly polarized antenna and a two-turn coil for UHF-RFID reader and NFC applications. In [2], the NFC square coil antenna was fabricated on the opposite side of the UHF RFID reader patch antenna for mobile phones. In [3], the authors proposed NFC loop antenna with nonuniform meandering lines and partial coverage ferrite sheet for metal-cover smartphone applications. The e-textile wearable NFC antenna integrated with garments using embroidery techniques was proposed in [4]. The near-field antennas for UHF RFID applications were designed and implemented in [5]–[8].

The multipolarized reader antennas for UHF RFID near-field applications were presented in [9], [10]. In [11], the authors proposed a printed dual-log-periodic dipole array antenna for UHF near-field RFID applications. In [12],

The associate editor coordinating the review of this manuscript and approving it for publication was Mohamed Kheir.

a load-integrated U-shaped near-field UHF RFID antenna array was proposed for a smart blood bag management system. In [13], a broadband low far-field gain antenna was presented for UHF RFID near-field applications. In [14], the elliptical antenna was designed for UHF wearable applications. A dual-band circularly polarized antenna was presented in [15] for UHF-RFID/WLAN applications.

In [16], a compact 0.92/2.45 GHz dual-band directional circularly polarized (CP) microstrip antenna was proposed for handheld RFID reader applications. In [17], a dual-band circularly polarized antenna was designed and implemented for UWB/UHF RFID applications. In [18], the authors proposed a hybrid passive UHF/UWB RFID antenna for passive indoor identification and localization systems. In [19], the integrated UWB-UHF antenna was designed using a single port for localization and energy harvesting. In [20], the authors proposed the circularly polarized square microstrip antenna for 2.45 GHz RFID applications. In [21], The square loop antenna with modified microstrip feed was designed and fabricated for near- and far-field RFID applications. In [22], the dual-band RFID tag antenna was designed using a series Hilbert-curve loop and matched stub for HF and UHF applications.

In [23], the authors proposed a planar compact multiple-input multiple-output (MIMO) antenna for IoT applications. The mutual coupling effect of the UHF RFID near-field tag antenna was presented in [24] for IoT environment. A compact 915 MHz antenna was fabricated and presented in [25] for future IoT wearable applications.

In [29], [30], the authors proposed antenna designs that utilize a simplified composite left/right-handed transmission line (SCRLH-TL) for ultrawideband (UWB) applications. In [31], the authors proposed a leaky-wave antenna that is capable of manipulating beam directions of the radiation pattern. The antenna with three asymmetric fork-shaped radiators for multiband and broadband communication applications was presented in [32]. In [33], a metamaterial electromagnetic bandgap structure was proposed to enhance isolation between transmit/receive radiating elements in densely packed array antennas of synthesis aperture radar (SAR) and multiple-input multiple-output (MIMO) systems. In [34] , a multiband antenna using periodic array of complementary artificial magnetic conductor metamaterial structure was proposed for broadband wireless transceivers.

In [35], the authors proposed a metamaterial transmission line structure to enhance the gain and radiation efficiency of antennas for multiple wireless communication applications. In [36], a leaky-wave antenna using metamaterial-based composite right/left-handed (CRLH) transmission lines was proposed for millimeter-wave applications. In [37], a metamaterial electromagnetic bandgap structure inserted between two closely spaced patch antennas was developed for mutual coupling reduction. In [38], the antennas based on metamaterial unit-cells were proposed for integration in UWB wireless communication systems and microwave portable devices. In [39], a planar broadband antenna using two pairs

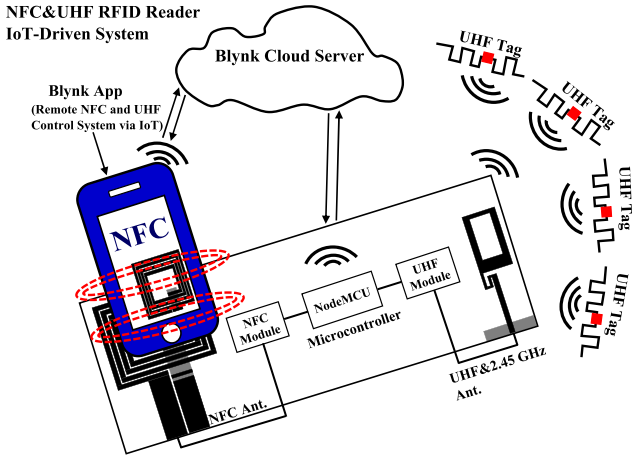

FIGURE 1. Diagram of IoT-linked integrated NFC near-field and far-field communication system board.

of meander line loops was realized for portable wireless communication devices. In [40], the authors proposed techniques to expand the impedance bandwidth of patch antennas for reliable multiband radio frequency (RF) communications.

The antennas are proposed in [1]–[22] for near- and far-field communication applications. However, the antennas in novel RFID system demand the integration of both near- and far-field operations into the same system. In addition, the antennas are designed and implemented in [23]–[25] for IoT applications. These antenna schemes do not utilize a node microcontroller unit and the mobile application on smartphone for IoT-linked near-and far-field communication.

This research proposes an integrated NFC and dual band UHF/2.45 GHz RFID reader antenna scheme for IoT applications. The integrated scheme utilizes a node microcontroller unit and the Blynk mobile app via smartphone. Simulations were carried out using CST Studio Suite, and prototype antennas were fabricated and integrated into the system board for near- and far-field communication via IoT. The integrated antenna scheme is proven ideal for IoT applications as it could achieve the NFC, UHF, and MW (2.45 GHz) frequency bands.

As shown in Fig. 1, the operating principle of the proposed integrated NFC and UHF RFID system board involves three modes: initiation, tag recognition, and termination modes. In the initiation mode, a command is sent from a user's smartphone using Blynk mobile application (Blynk App) via coupled magnetic field by hovering the smartphone above the NFC antenna of the board system; and the system board verifies universal identification (UID) of the NFC tag embedded in the smartphone against data stored in the microcontroller with Wi-Fi module (NodeMCU).

In the tag recognition mode, the NFC module reads the information in the NFC tag via short-distance contactless data transmission, and the UHF RFID module reads the information in the UHF RFID tag using radio frequency electromagnetic field. The tag recognition mode concurrently executes the NFC and UHF RFID functions and transfers data

TABLE 1. The dimensions of the modified NFC antenna.

Parameters	W_X	L_X	W_1	W_2	W_3	W_4	W_5	W_6	W_7	W_8	W_9
Unit (mm)	70	100	66	58	50	42	36	13	13	5	13
Parameters	W_{10}	L_1	L_2	L_3	L_4	L_5	L_6	L_7	L_8	L_9	L_{10}
Unit (mm)	13	52	44	36	28	5	39	37	35	40	60

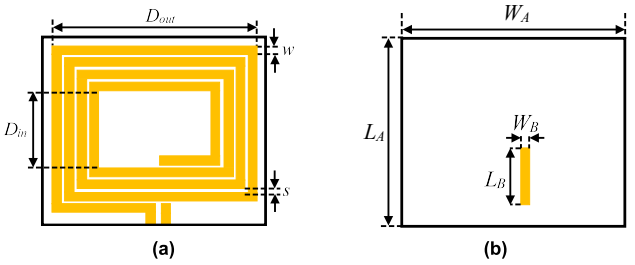

FIGURE 2. The initial NFC antenna: (a) front view, (b) rear view.

to a cloud server (Blynk cloud server) via Internet of Things (IoT). To retrieve the data, the user sends a command to the cloud server via Blynk App and the cloud server will forward the command to the microcontroller. Upon receiving the command, the NFC and UHF RFID modules which are serially connected to the microcontroller read the UID of NFC and UHF RFID tags. The UID and corresponding data are then briefly retained in the internal memory of the microcontroller before forwarding to the cloud server via IoT. The data (both real-time and archival) are viewable on the smartphone using Blynk app via IoT.

In the termination mode, the user (i.e., one who initiates the system) sends another command via Blynk mobile application by hovering the smartphone above the NFC antenna to terminate the system.

II. EVOLUTION OF THE INTEGRATED ANTENNA SCHEME

A. NFC ANTENNA STRUCTURE

Fig. 2 illustrates the initial NFC antenna of planar square spiral loops, operable at 13.56 MHz. The initial antenna has four turns with inner (D_{in}) and outer diameters (D_{out}) of 56 mm and 66 mm. The strip width (w) is 3 mm and the gap between strips (s) is 1 mm. The antenna is printed on an FR-4 substrate with a relative permittivity and loss tangent of 4.4 and 0.02. The overall dimension of the initial NFC antenna is 70 mm × 64 mm ($W_A \times L_A$).

To realize the impedance matching, the planar square spiral loops of the initial NFC antenna were redesigned. The modified NFC antenna is of planar square spiral loops with four turns and a feed line. Figs. 3(a)-(b) depict the geometry (front and rear) of the modified NFC antenna, and Fig. 3(c) compares the simulated $|S_{11}|$ of the initial and modified NFC antennas, demonstrating that the modified NFC antenna achieves the impedance matching ($|S_{11}| < -10$ dB) at 13.56 MHz. Table 1 tabulates the dimensions of the modified NFC antenna.

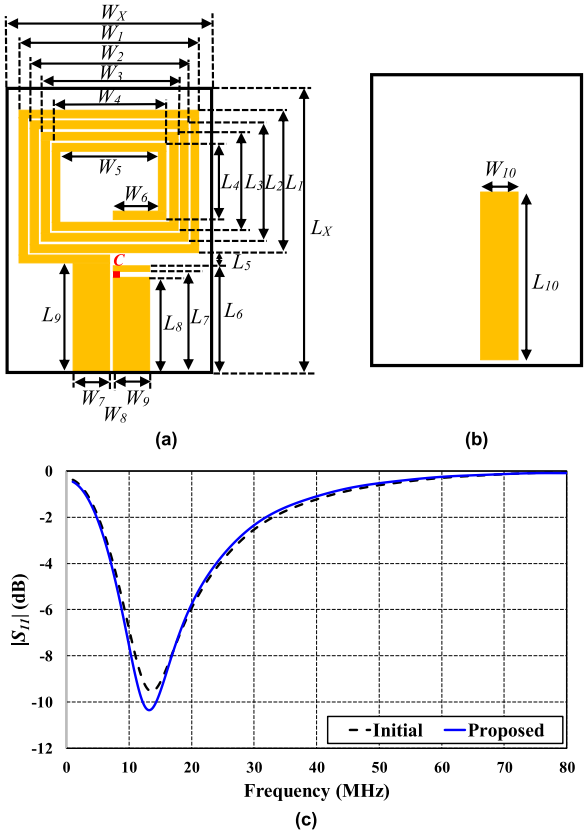

FIGURE 3. The modified NFC antenna: (a) front view, (b) rear view, (c) simulated $|S_{11}|$ of the initial and modified antennas.

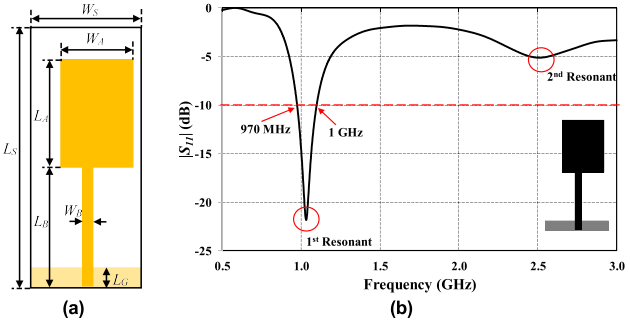

FIGURE 4. The initial rectangular monopole antenna: (a) the antenna geometry, (b) simulated $|S_{11}|$.

B. DUAL BAND UHF/2.45 GHz READER ANTENNA STRUCTURE

Fig. 4(a) shows the geometry of initial rectangular monopole antenna, consisting of a radiating element, a feed line, and

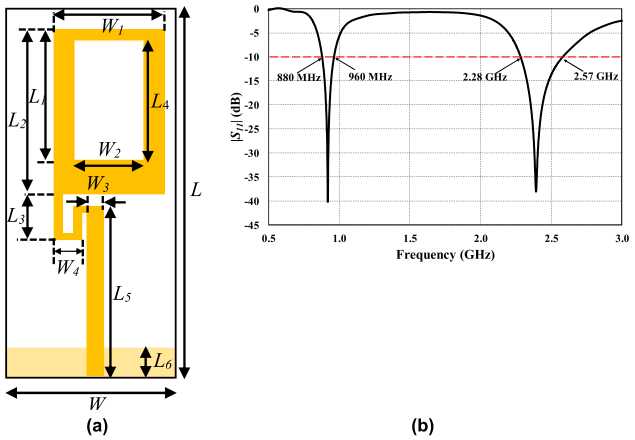

FIGURE 5. The dual band UHF/2.45 GHz RFID reader antenna: (a) the antenna geometry, (b) simulated $|S_{11}|$.

a ground plane. The radiating element and the feed line are printed on top of an FR-4 substrate whose thickness, permittivity, and loss tangent are 1.6 mm, 4.4, and 0.02. The ground plane is printed on the rear of the substrate. The dimensions of the radiating element and the feed line are 27 mm × 40 mm ($W_A \times L_A$) and 4 mm × 44 mm ($W_B \times L_B$), respectively. The ground plane of the initial monopole antenna is 41 mm × 7.5 mm ($W \times L$) in dimension. The overall dimension of the initial monopole antenna is 55 mm × 55 mm ($W_s \times L_s$). The antenna could achieve the dual band UHF (920-925 MHz) and 2.45 GHz RFID frequency band.

In Fig. 4(b), there are two resonance frequencies. The simulated impedance bandwidth ($|S_{11}| < -10$ dB) of the first resonance covers 970 MHz - 1GHz, while the second resonance fails to realize impedance matching at 2.45 GHz. Besides, the first resonance suffers from the resonant frequency mismatch as it falls outside of the target UHF RFID band. Therefore, the initial monopole antenna requires further refinement to realize the dual-band UHF and 2.45 GHz RFID bands.

To realize the dual-band frequencies with broad impedance bandwidth, a rectangular-shaped slot was etched into the radiating element, and the feed line was augmented with a meander line. The ground plane is on the rear of the FR-4 substrate. The overall dimension of the refined monopole antenna is 41 mm × 100 mm × 1.6 mm, as shown in Fig. 5(a). Table 2 tabulates the dimensions of dual band UHF/2.45GHz RFID reader antenna.

In Fig. 5(b), the simulated impedance bandwidth ($|S_{11}| < -10$ dB) of the first and second resonance of the refined monopole antenna cover 880 MHz - 960 MHz and 2.28 GHz – 2.57 GHz. Both resonance frequencies realize a broad impedance bandwidth covering the UHF and MW (2.45 GHz) bands, rendering it suitable for UHF/2.45 GHz RFID applications.

III. PARAMETRIC ANALYSIS

A. MODIFIED NFC ANTENNA

Fig. 6(a) compares the simulated $|S_{11}|$ of the modified NFC antenna under different feed line lengths (6, 25, and 40 mm).

TABLE 2. The dimensions of the dual band UHF/2.45 GHz RFID reader antenna.

Parameters	*W*	*L*	*W1*	*W2*	*W3*	*W4*
Unit (mm)	41	100	27	17.5	4	6.8
Parameters	*L1*	*L2*	*L3*	*L4*	*L5*	*L6*
Unit (mm)	32	40	11	29	41	7.5

As the length of the feed line increases, the impedance matching approaches −10 dB or lower. In this research, the optimal feed line length of the modified NFC antenna is 60 mm.

Fig. 6(b) illustrates the simulated $|S_{11}|$ of the modified NFC antenna under variable ground strip lengths (24, 40, and 60 mm). As the ground strip length increases, given the ground strip width of 13 mm, the impedance matching approaches −10 dB or lower. The optimal ground strip width and length of the NFC antenna are 13 mm and 60 mm.

Fig. 6(c) demonstrates the simulated $|S_{11}|$ of the NFC antenna under various capacitances of the capacitive lumped element (50, 100, and 150 pF). The capacitance of the capacitive lumped element affects the resonance frequency. As the capacitance increases from 50pF to 150pF, the resonance frequency is shifted leftward. The impedance bandwidths at 50 pF and 100pF fail to cover the target NFC frequency band. Thus, the optimal capacitance is 150 pF.

B. DUAL BAND UHF/2.45 GHz READER ANTENNA

Fig. 7(a) illustrates the simulated $|S_{11}|$ of the refined monopole antenna under various meander turns ($N = 0, 1, 2$). The number of meander turns affects the resonance frequency and impedance bandwidth of the UHF and 2.45 bands. Under $N = 0$, the antenna suffers a resonant frequency mismatch at the UHF RFID band and fails to achieve impedance matching at the 2.45 GHz RFID band.

As the meander turn increases from 0 to 2, the lower and higher frequencies are shifted leftward, resulting in a decrease in impedance bandwidth. With one meander turn ($N = 1$), the UHF operating frequency range is 0.88-0.96 GHz (8.69%) and that of MW is 2.28-2.57 GHz (11.96%). With $N = 2$, the UHF operating frequency range is 0.83-0.90 GHz (7.47%) and that of MW is 2.25-2.41 GHz (7.08%). The number of meander turns and the bandwidth are inversely correlated. Specifically, the bandwidth decreases with increase in meander turn. In this research, the optimal meander turn of the refined monopole antenna is 1. With $N = 1$, the impedance bandwidths at 920 MHz and 2.45 GHz resonant frequency are −40.85 dB and −44.67 dB.

Fig. 7(b) compares the simulated $|S_{11}|$ of the refined monopole antenna under different slot patterns: E, L, T, and rectangular slot patterns. The slot pattern has an effect on the impedance bandwidth and resonant frequency of the MW band. At 920 MHz, the impedance bandwidths of E, L, T slotted antennas are −23.56 dB, −23.81 dB, and −42.40 dB, with the identical resonant frequency of 910 MHz. At 2.45 GHz, the corresponding impedance bandwidths are −14.00 dB, −4.15 dB, and −17.15 dB, with the respective resonant

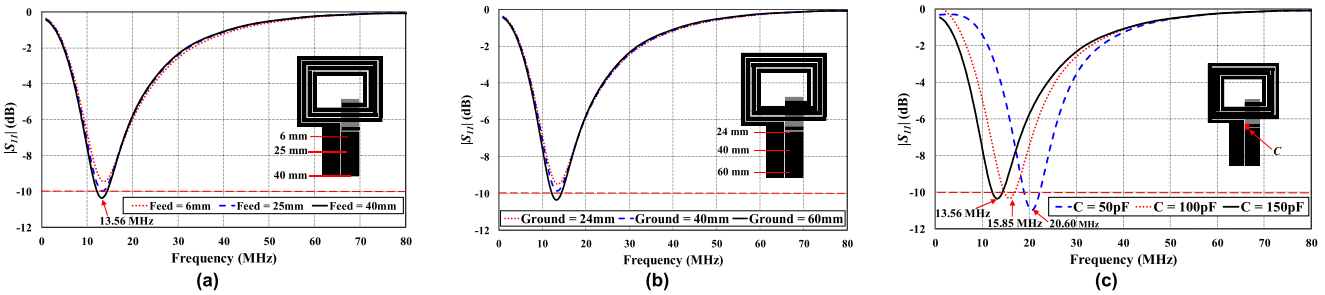

FIGURE 6. Simulated $|S_{11}|$ of the NFC reader antenna under variable: (a) feeding lengths, (b) ground strip lengths, (c) capacitance of the capacitor.

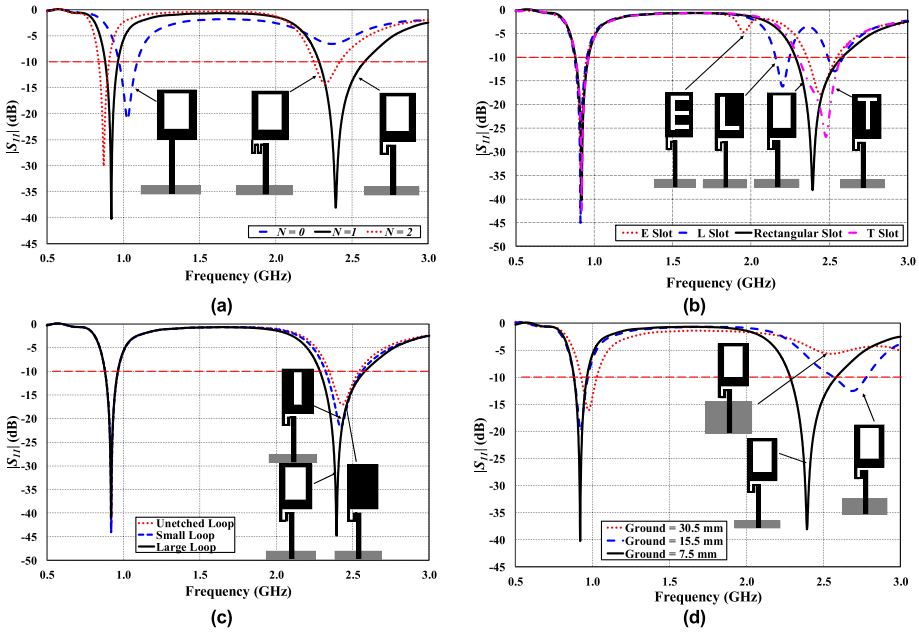

FIGURE 7. Simulated $|S_{11}|$ of the dual band UHF/2.45 GHz antenna under variable: (a) meander turns, (b) slot patterns, (c) slot widths, (d) ground strip lengths.

frequencies of 2.44 GHz, 2.20 GHz, and 2.47 MHz. The results show that the first resonance is insensitive to the slot pattern, while the second resonance is noticeably affected by slot pattern. The optimal slot pattern is the rectangular pattern, achieving the impedance bandwidths of −40.85 dB at 920 MHz and −44.67 dB at 2.45 GHz.

Fig. 7(c) demonstrates the simulated $|S_{11}|$ of the monopole antenna under different slot widths (0, 8, 18 cm). The slot widths have an effect on the bandwidth, impedance bandwidth, and resonant frequency of the MW band. The slot widths are positively correlated with the bandwidth. Specifically, the MW bandwidth increases (9.83% to 11.96%) with increase in slot width. On the other hand, the impedance bandwidth shifts from −20.14 dB to −44.85 dB as the slot width increases. The results revealed that the impedance matching of UHF RFID frequency (920-925 MHz) is independent of slot widths. On the other hand, the impedance matching at the 2.45GHz band is significantly improved with increase in the slot width.

Fig. 7(d) illustrates the simulated $|S_{11}|$ of the monopole antenna under variable ground strip lengths (7.5, 15.5, 30.5 mm), given the width of 41 mm. The ground strip length has an effect on the bandwidth, impedance bandwidth, and resonant frequency of the UHF and MW bands. With 30.5 mm ground stirp, the first resonance fails to cover the UHF band, and the second resonance ($|S_{11}|$) is far above −10 dB. With 15.5 mm ground strip, the first resonance is shifted to a lower frequency and an impedance mismatch occurs at the second resonance. The antenna achieves the dual-band UHF/MW frequency as the ground strip length is reduced from 30.5 to 7.5 mm. The MW bandwidth increases from 7.88% to 11.96% as the ground strip length is shortened from 30.5 to 7.5 mm. The optimal ground strip length is 7.5 mm.

In essence, the resonant response of the refined monopole antenna (UHF/2.45GHz antenna) is governed by the meander turns, slot pattern, slot width, and ground plane dimension.

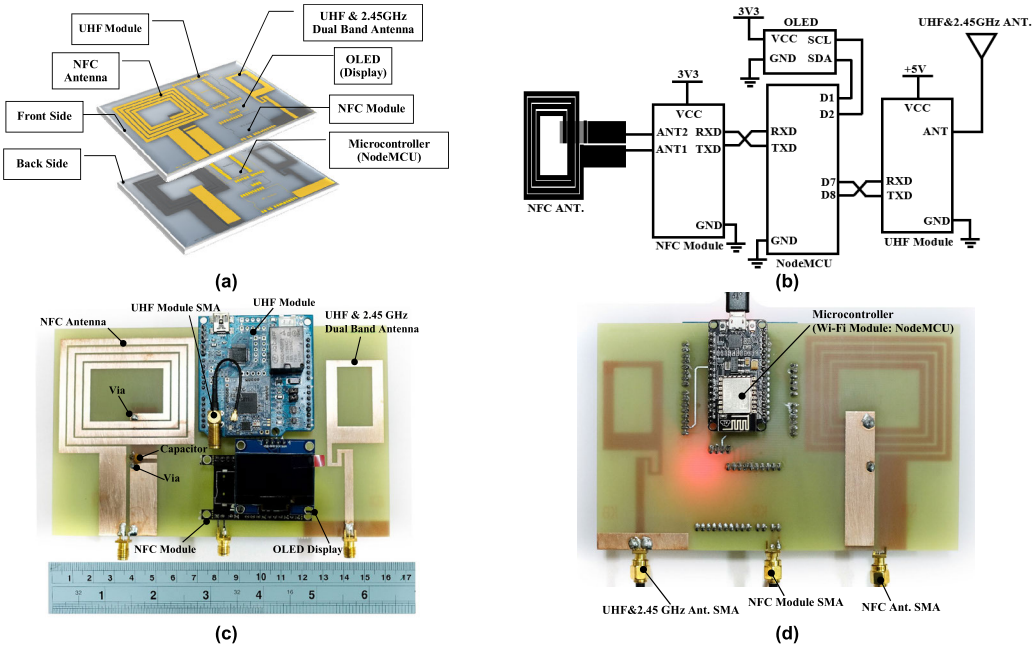

FIGURE 8. The integrated NFC and dual band UHF/2.45 GHz antenna scheme: (a) 3D perspective view, (b) schematic of the integrated antenna, (c) front view, (d) rear view of the prototype antenna.

IV. INTEGRATED NEAR AND FAR FIELD COMMUNICATION SYSTEM

A. CIRCUIT MODELLING OF NFC AND DUAL BAND UHF/2.45 GHz RFID SYSTEM

Figs. 8 (a)-(b) illustrate the 3D perspective view and the schematic of the integrated NFC and dual band UHF/2.45GHz RFID antenna scheme (i.e., integrated RFID antenna scheme) for near- and far-field communication. Data are stored in a cloud server accessible via the internet using a mobile application on smartphone, i.e., the Internet of Things (IoT).

Figs. 8(c)-(d) depict the front and rear views of a prototype of the system board of integrated RFID antennas for IoT applications. The overall dimension of the system board is 100mm $\times$ 160mm $\times$ 1.6mm. The integrated antenna scheme is made up of three components: hardware, software, and mobile application.

The hardware consists of an NFC reader module, UHF reader module, organic light emitting diode (OLED) display, NFC antenna, dual band UHF/2.45 GHz antenna, and a microcontroller of ESP8266 chip with built-in Wi-Fi module (NodeMCU). The NodeMCU communicates and controls the NFC module, UHF module, and OLED display. The NFC and UHF modules are connected serially, and the display is connected to an inter-integrated circuit (I2C). The NFC reader module contains PN532 chip (Smartfly Technology) [26] and supports ISO/IEC 18000-3 standard. The UHF reader module is of AS3992 protocol (ElecKits Technologies) [27] and supports RFID EPC Gen2 and ISO18000-6C/6B standards.

An algorithmic scheme (the software) embedded in the microcontroller is used to control the OLED display, NFC module, and UHF module; and to interface with the mobile application on smartphone. Specifically, the mobile application is the Blynk app, which is a graphical user interface (GUI) compatible with both iOS and Android. The mobile app interacts with the cloud server, and instructions are transmitted via the internet to the system board.

B. IoT-LINKED NEAR AND FAR FIELD COMMUNICATION SYSTEM

In the operation, an NFC tag in a smartphone or a UHF tag embedded in a card is placed or hovered above the system board where universal identification (UID) data are read by the NFC or UHF module. The UID data are processed in the NodeMCU and transmitted to the cloud server using the Blynk mobile application. The Blynk app is capable of simultaneous execution of NFC and UHF RFID systems. The data stored in the cloud server are viewable on the mobile screen and can be graphically rendered (both archival and real time) using the Blynk app.

V. SIMULATED AND MEASURED RESULTS

A. NFC ANTENNA

Fig. 9(a) presents the simulated input impedance of the NFC antenna. The real and imaginary input impedance indicate an input resistance and reactance of 93.67 Ohm and j2.35 Ohm. The input reactance also exhibits an inductive behavior. In Fig. 9(b), the simulation and measured results are agreeable, and the NFC antenna resonates at 13.56 MHz.

Fig. 10 illustrates the magnetic field distribution of the NFC antenna, dividing into three distinct areas by intensity. The first area is on the left and right loops of the planar spiral

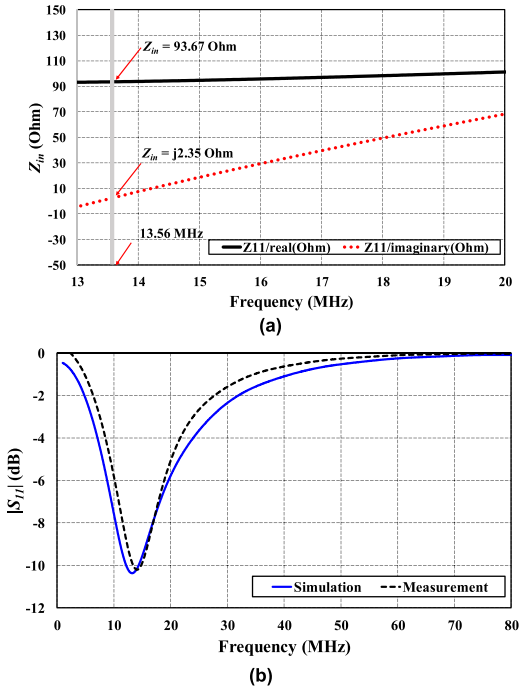

FIGURE 9. The NFC reader antenna: (a) simulated input impedance, (b) simulated and measured $|S_{11}|$.

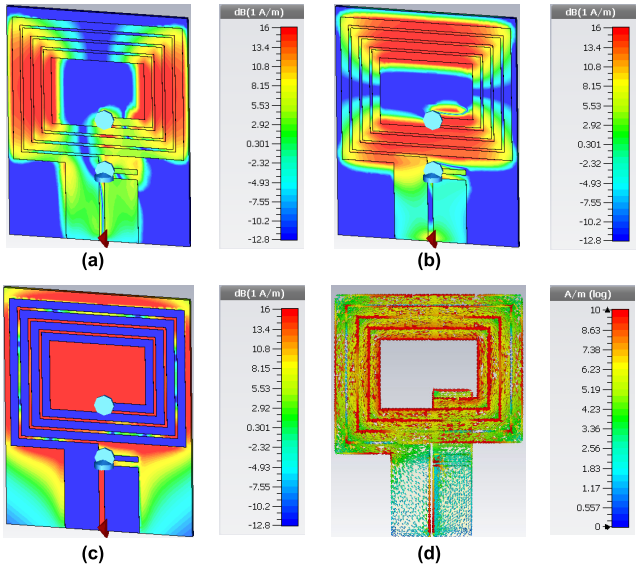

FIGURE 10. Magnetic field distribution of the NFC antenna at 13.56 MHz: (a) H_x, (b) H_y, (c) H_z, (d) simulated current distribution.

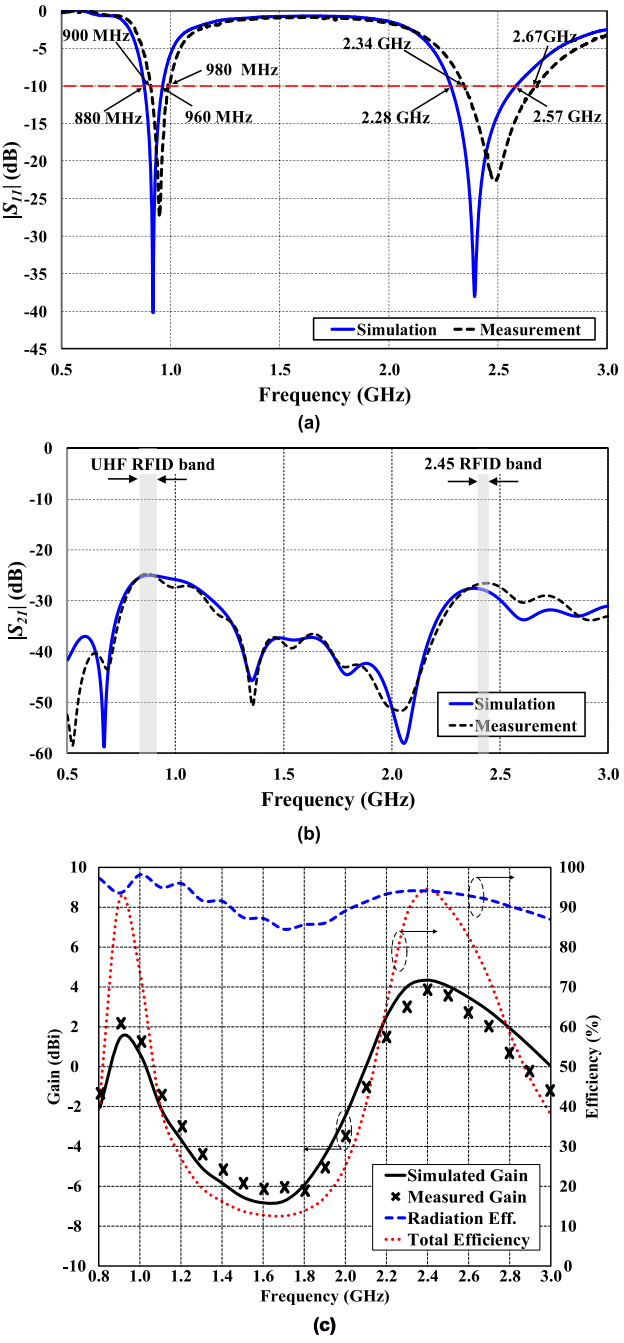

FIGURE 11. Simulated and measured results of the dual band UHF/2.45 GHz RFID antenna: (a) $|S_{11}|$, (b) $|S_{21}|$ (c) radiation, total efficiency and gains.

coil (Fig. 10(a)). The second area is on the top and bottom loops of the spiral coil (Fig. 10(b)), and the final area is on the rear of the planar spiral coil, as shown in Fig. 10(c).

Fig. 10(d) demonstrates the simulated distribution of surface current along the planar square spiral loops and feed line of the NFC antenna at 13.56 MHz. The surface current is present on four loops of the planar spiral coil. The current flows from the feeding point along the feed line to the outermost and innermost loops through to the ground strip and the capacitive lumped element. The strong current along the edges of the loops induces magnetic fields in the near field region, and the current along the feed line through to the ground strip generates electric and magnetic fields in the far field region.

B. DUAL BAND UHF/2.45 GHz RFID READER ANTENNA

Fig. 11(a) shows the simulated and measured $|S_{11}|$ of the dual band UHF/2.45GHz antenna. The simulated $|S_{11}|(< \ -10$ dB) covers the UHF (880-960 MHz) and MW bands (2.28-2.57 GHz), with 8.69% and

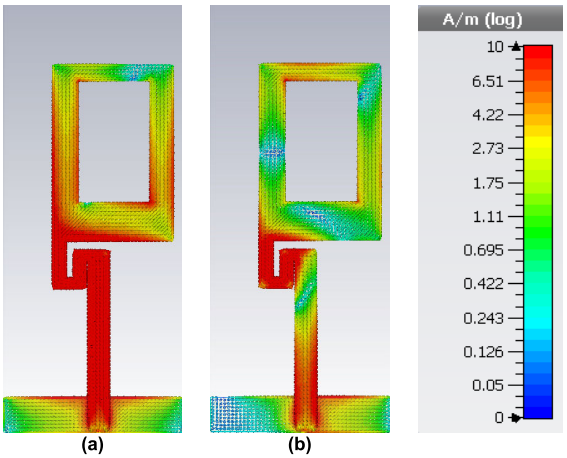

FIGURE 12. Simulated current distribution at: (a) 0.92 GHz, (b) 2.45 GHz.

11.96% bandwidth, respectively. The measured $|S_{11}|$ covers the UHF (900-980 MHz) and MW bands (2.34-2.67 GHz), with 8.51% and 13.20% bandwidth. The simulated and measured results are in good agreement, indicating that the antenna achieves both UHF and MW bands with high isolation.

The simulated and measured $|S_{21}|$ of the UHF band are −25.19 dB and −26.94 dB, and the corresponding $|S_{21}|$ of 2.45 GHz RFID band are −27.63 dB and −26.72 dB, as illustrated in Fig. 11(b). The simulated and measured $|S_{21}|$ of the UHF and 2.45 GHz RFID bands are in the range from −28 to −25 dB, thus satisfactorily achieving isolation between NFC and UHF/2.45 GHz RFID reader antenna ports [1], [15].

Fig. 11(c) illustrates the simulated and measured antenna gains over the UHF (920-925 MHz) and MW (2.45 GHz) bands. The maximum simulated and measured gains are 4.37 and 3.97 dBi over the 2.45 GHz frequency band. The simulated radiation and total efficiency over the UHF band are 94.36% and 92.05%, and those of 2.45 GHz band are 94.85% and 94.81%.

Figs. 12 (a)-(b) illustrate the simulated surface current distribution of the dual band UHF/2.45GHz antenna using CST Microwave Studio Suite [28] at the lower (920 MHz) and higher frequency (2.45 GHz). In Fig. 12(a), at the lower frequency, the current is noticeably strong along the feeding point, feeding line, and meander line, but dissipates as it travels along the lower edge of the loop radiator. The current then travels along the loop from left to right before arriving at the ground plane. In Fig. 12 (b), at the higher frequency, the current is strong around the feeding point, meander line, and the upper edge of the ground plane, while the loop radiator exhibits moderate amounts of current.

Table 3 summarizes the simulated and measured results of the dual band UHF/2.45 GHz antenna. With the optimal antenna dimensions, the simulated $|S_{11}|$ at 920MHz, 925 MHz, and 2.45 GHz are −40.85 dB, −27.74 dB, and −44.67 dB, with the simulated bandwidths of 8.69% over UHF band and 11.96% over the

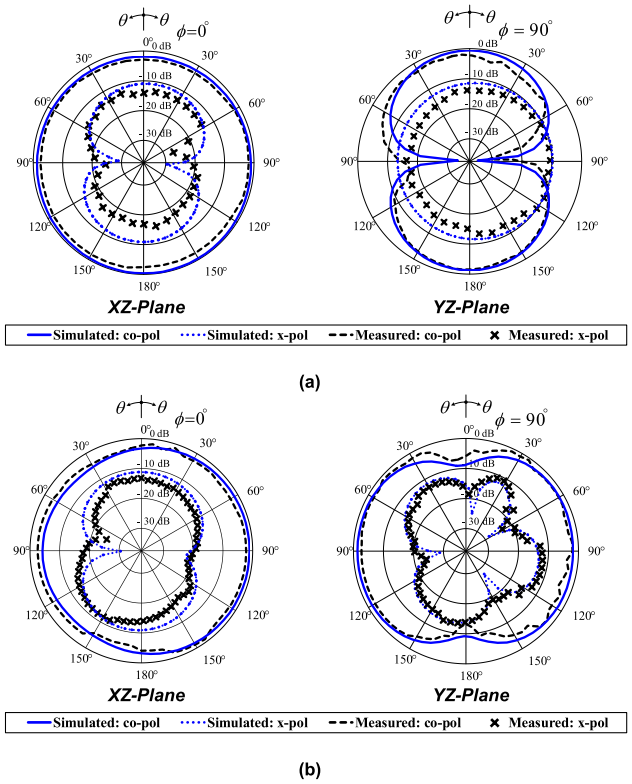

FIGURE 13. Radiation patterns of the dual band UHF/2.45GHz antenna: (a) 920 MHz, (b) 2.45 GHz.

MW band. The corresponding measured $|S_{11}|$ are −12.58 dB, −14.12 dB, and −14.45 dB, with the measured bandwidths of 8.51% over UHF band and 13.20% over the MW band.

Fig. 13 illustrates the simulated and measured radiation patterns of the dual band UHF/2.45GHz antenna at 920 MHz (UHF band) and 2.45 GHz (MW band) along the *xz* and *yz* planes. The simulation and measurement results are in good agreement. The simulated and measured radiations in the *xz* and *yz* planes are near-omnidirectional for both frequencies. The maximum simulated and measured cross polarizations (*x-pol*) are approximately −10 dB in the *xz* and *yz* planes. At the lower frequency, the co-polarization of the *xz* and *yz* planes are nearly symmetrical. However, at the higher frequency, the *yz*-plane cross polarization is disturbed.

A typical UHF RFID reader antenna is of circular polarization (CP). Nonetheless, to achieve consistent reading between the tag and the UHF module, the UHF RFID reader antenna of this research is deliberately designed to be linear polarized (LP). In addition, an antenna with directional radiation pattern is preferable for UHF RFID reader applications. Despite shorter reading ranges, the near-omnidirectional radiation pattern of this work can recognize UHF RFID tags in all directions due to its wide coverage.

C. READING RANGE OF IoT-LINKED INTEGRATED NFC AND UHF RFID SYSTEM

The reading test of NFC and UHF RFID reader antennas was undertaken using the system board prototype, as shown

TABLE 3. Simulated and measured results of the dual band UHF/2.45 GHz antenna.

Characteristic	Simulation Results					
	Meander turn = 0	Meander turn = 2	E Slot	L Slot	T Slot	Initial (unetched) monopole antenna
UHF band (GHz)	0.97-1.08	0.83-0.90	0.88-0.95	0.87-0.95	0.88-0.96	0.88-0.96
MW band (GHz)	–	2.25-2.41	2.35-2.54	2.49-2.58	2.3-2.57	2.34-2.54
BW of UHF (%)	10.32	7.47	7.80	8.79	8.69	8.69
BW of MW (%)	–	7.08	7.77	3.55	11.09	8.19
UHF Resonant Freq. (GHz)	1.02	0.87	0.91	0.91	0.91	0.92
MW Resonant Freq. (GHz)	–	2.32	2.44	2.20	2.47	2.43
$\|S_{11}\|$ at 920MHz (dB)	-4.95	-7.36	-23.56	-23.81	-42.40	-37.67
$\|S_{11}\|$ at 925MHz (dB)	-5.31	-6.69	-19.40	-19.65	-29.15	-31.77
$\|S_{11}\|$ at 2.45 GHz (dB)	-6.45	-10.84	-14.00	-4.15	-17.15	-15.48

Characteristic	Simulation Results				Measured results under optimal dimensions
	Small Loop	Ground = 30.5 mm	Ground = 15.5 mm	Simulated results under optimal dimensions	
UHF band (GHz)	0.88-0.96	0.92-1.02	0.88-0.96	0.88-0.96	0.90-0.98
MW band (GHz)	2.32-2.56	–	2.56-2.77	2.28-2.57	2.34-2.67
BW of UHF (%)	8.69	10.23	8.69	8.69	8.51
BW of MW (%)	9.83	–	7.88	11.96	13.20
UHF Resonant Freq. (GHz)	0.92	0.97	0.92	0.92	0.95
MW Resonant Freq. (GHz)	2.42	–	2.68	2.40	2.48
$\|S_{11}\|$ at 920MHz (dB)	-43.93	-9.20	-19.91	-40.85	-12.58
$\|S_{11}\|$ at 925MHz (dB)	-29.76	-9.85	-20.00	-27.74	-14.12
$\|S_{11}\|$ at 2.45 GHz (dB)	-20.14	–	-6.36	-44.67	-14.45

in Fig. 14. Due to the unavailability of 2.45 GHz RFID module, the reading experiments were confined to NFC and UHF RFID systems.

Fig. 14(a) illustrates the reading experiment between the on-board NFC reader antenna and the NFC tag antenna embedded in the smartphone via the Blynk mobile app. In Fig. 14(b), the NFC tag antenna is attached to a computer numerical control (CNC) machine in the *xy* plane for near-field measurement, and the reading performance between the tag and the on-board NFC reader antenna is determined.

In Fig 14(c), the NFC tag-embedded smartphone is hovered over the on-board NFC reader antenna at variable distances: 1, 2, 3, and 4 cm. In addition, the NFC tag is motioned in 1 cm increment in all directions inside an 8 cm × 10 cm test area, comprising 80 grid cells (1 cm × 1 cm). Both the NFC reader antenna and the tag are initially at the center of the test area. Fig. 14(d) demonstrates the reading results on the smartphone display.

In UHF reading test, the integrated system board is placed on polyurethane (PU) foam block in *xy* plane with a height of 1 m from the ground, and a 860-960MHz UHF passive RFID tag card (Alien 9654 Inlay) is placed on another PU foam block directly opposite to the system board in an anechoic chamber (Fig. 14(e)). The distances between the board and the tag card were varied between 60, 120, 240, and 300 cm. The reading performance of the UHF RFID tag is inversely correlated to the distance. In other words, the reading performance decreases with increase in the distance.

Table 4 compares between the proposed integrated NFC and dual-band UHF/2.45 GHz antennas and existing antennas of similar functionality. The comparison encompasses

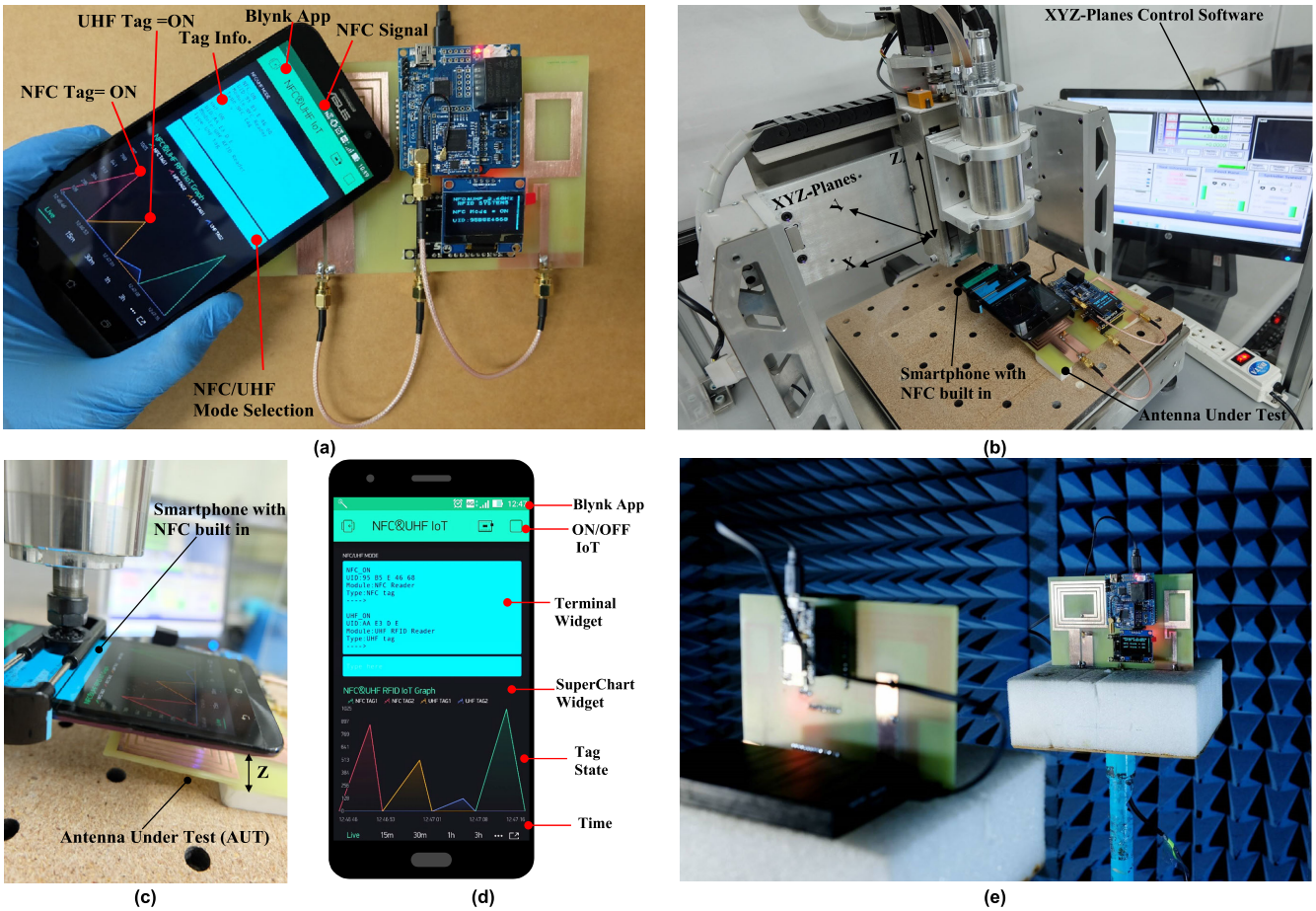

FIGURE 14. The reading performance of IoT-linked integrated system board: (a) reading experiment between NFC reader and tag antennas, (b) NFC tag antenna attached to CNC machine, (c) NFC reading test, (d) reading results by Blynk app on smartphone, (e) UHF far-field reading experiment.

TABLE 4. Performance comparison of the proposed NFC and UHF/2.45 GHz RFID reader antenna and applications with recent literature.

Ref.	Dimension (mm^3)	Application				Operating Freq. /Bandwidth			$\|S_{11}\|$ (dB)		Max. Gain (dBi)	Polarization
		NFC	UHF RFID	IoT	Smart phone	HF (MHz)	UHF (GHz)	MW (GHz)	UHF	MW		
[1]	150×110 ×1	–	–	–	–	13.56	0.78-1.07 (31.35%)	–	-40	–	3.4	Circular
[2]	60×100 ×0.8	√	√	–	–	13.56	0.85-0.87 (2.31%)	–	-23	–	-3.7	Linear
[8]	480×200 ×1	–	√	–	–	–	0.914-0.929 (1.63%)	–	-32	–	N/A	Linear
[11]	170×170 ×1	–	√	–	–	–	0.824-0.953 (14.5%)	–	-40	–	N/A	N/A
[16]	110×110 ×6.6	–	√	–	–	–	0.903-0.938 (3.8%)	2.18-2.59 (17.2 %)	-30	-22	8.9	Circular
This work	**100×160 ×1.6**	√	√	√	√	**13.56**	**0.88-0.96 (8.69%)**	**2.28-2.57 (11.96%)**	**-40.8**	**-44.6**	**4.37**	**Linear**

the operating frequency, bandwidth, impedance bandwidth, gain, polarization, dimension, and applications. The proposed scheme integrates NFC and dual-band UHF/2.45 GHz RFID reader antennas that are applicable to near- and far-field wireless communication. The novelty of the proposed integrated antennas lies in the use of cloud technology (i.e., IoT technology) to store real-time and archival data in place of traditional servers.

Figs. 15(a)-(d) compare the measured reading performance between the NFC reader and tag antennas at variable positions and hovering distances: 1, 2, 3, and 4 cm. The black and white grid cells represent readable and

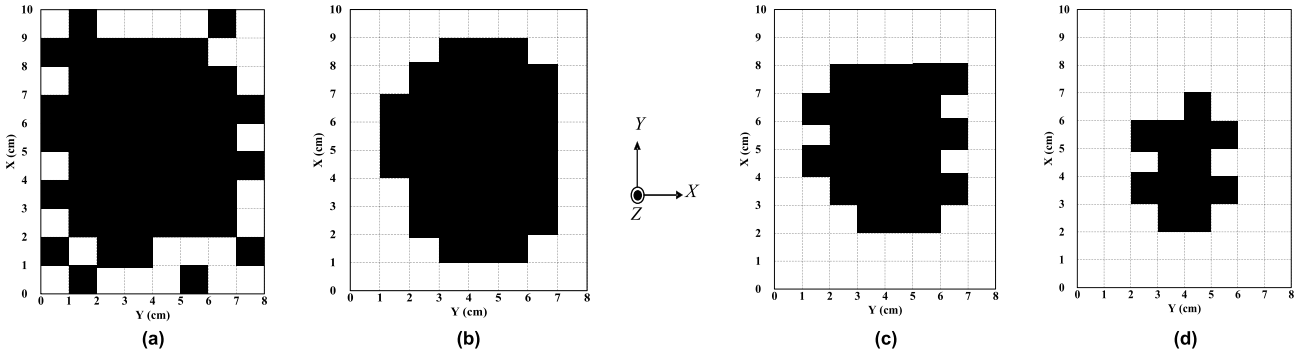

FIGURE 15. Measured readable areas between NFC reader and tag antennas at different hovering distances: (a) 1 cm, (b) 2 cm, (c) 3 cm, (d) 4 cm.

unreadable areas, respectively. The NFC reading performance worsens as the NFC tag is horizontally and vertically motioned away from the NFC reader antenna.

VI. CONCLUSION

This research proposed a system board of IoT-linked integrated antenna scheme of near-field communication (NFC) and dual band UHF (920-925 MHz)/2.45 GHz radio frequency identification (RFID) reader antennas. The integrated scheme utilizes a node microcontroller unit (Node-MCU) and the Blynk mobile app via IoT technology. In the antenna development, simulations were carried out using CST Studio Suite, and prototype antennas were fabricated and integrated into the system board for IoT-linked near- and far-field communication. The simulated $|S_{11}|$ of the integrated system board covers the UHF (880-960 MHz) and MW bands (2.28-2.57 GHz), with 8.69% and 11.96% bandwidth, and the measured $|S_{11}|$ covers the UHF (900-980 MHz) and MW bands (2.34-2.67 GHz), with 8.51% and 13.20% bandwidth. The NFC reader antenna resonates at 13.56 MHz, and the dual band UHF/2.45 GHz RFID reader antenna achieves the 920-925 MHz and MW bands with high isolation. The integrated antenna scheme satisfies the NFC, UHF, and MW frequency requirements, making it suitable for IoT applications.

REFERENCES

[1] M.-S. Wang, Y.-X. Guo, and W. Wu, "Planar shared antenna structure for NFC and UHF-RFID reader applications," *IEEE Trans. Antennas Propag.*, vol. 65, no. 10, pp. 5583–5588, Oct. 2017.
[2] F. Paredes, I. Cairo, S. Zuffanelli, G. Zamora, J. Bonache, and F. Martin, "Compact design of UHF RFID and NFC antennas for mobile phones," *IET Microw., Antennas Propag.*, vol. 11, no. 7, pp. 1016–1019, May 2017.
[3] J. Q. Zhu, Y. L. Ban, C. Y. D. Sim, and G. Wu, "NFC antennas with nonuniform meandering line and partial coverage ferrite sheet for metal cover smartphone applications," *IEEE Trans. Antennas Propag.*, vol. 65, no. 6, pp. 2827–2835, Jun. 2017.
[4] Y. Jiang, L. Xu, K. Pan, T. Leng, Y. Li, L. Danoon, and Z. Hu, "e-textile embroidered wearable near-field communication RFID antennas," *IET Microw., Antennas Propag.*, vol. 13, no. 1, pp. 99–104, Oct. 2018.
[5] Z. Xing, L. Wang, C. Wu, and K. Wei, "Study of broadband near-field antenna for ultra-high-frequency radio frequency identification applications," *IET Microw., Antennas Propag.*, vol. 5, no. 14, pp. 1661–1669, Aug. 2011.
[6] X. Qing, C. K. Goh, and Z. N. Chen, "A broadband UHF near-field RFID antenna," *IEEE Trans. Antennas Propag.*, vol. 58, no. 12, pp. 3829–3838, Dec. 2010.
[7] A. Ren, C. Wu, Y. Gao, and Y. Yuan, "A robust UHF near-field RFID reader antenna," *IEEE Trans. Antennas Propag.*, vol. 60, no. 4, pp. 1690–1697, Apr. 2012.
[8] Y. Yao, C. Cui, J. Yu, and X. Chen, "A meander line UHF RFID reader antenna for near-field applications," *IEEE Trans. Antennas Propag.*, vol. 65, no. 1, pp. 82–91, Jan. 2017.
[9] Y. Yao, Y. Liang, J. Yu, and X. Chen, "Design of a multipolarized RFID reader antenna for UHF near-field applications," *IEEE Trans. Antennas Propag.*, vol. 65, no. 7, pp. 3344–3351, May 2017.
[10] Y. Yao, X. Ren, Y. Liang, J. Yu, and X. Chen, "Multipolarized reader antenna with periodic units based on electric field coupling for UHF RFID near-field applications," *IEEE Trans. Antennas Propag.*, vol. 67, no. 8, pp. 5265–5271, Aug. 2019.
[11] H. Li, Y. Chen, Z. Xing, and S. Yang, "A novel printed dual-log-periodic array antenna for UHF near-field RFID applications," *IEEE Trans. Antennas Propag.*, vol. 66, no. 12, pp. 7418–7423, Dec. 2018.
[12] M. G. Jeong and W. S. Lee, "A smart blood bag management system using a load-integrated U-shaped near-field RFID antenna array," *IEEE Trans. Antennas Propag.*, vol. 67, no. 3, pp. 1837–1843, Mar. 2019.
[13] Y. Yao, Y. Liang, J. Yu, and X. Chen, "A broadband near-field UHF RFID reader antenna with low far-field gain," *IEEE Trans. Antennas Propag.*, vol. 65, no. 9, pp. 4869–4874, Sep. 2017.
[14] G. A. Casula, G. Montisci, G. Valente, and G. Gatto, "A robust printed antenna for UHF wearable applications," *IEEE Trans. Antennas Propag.*, vol. 66, no. 8, pp. 4337–4342, Aug. 2018.
[15] R. Caso, A. Michel, M. Rodriguez-Pino, and P. Nepa, "Dual-band UHF-RFID/WLAN circularly polarized antenna for portable RFID readers," *IEEE Trans. Antennas Propag.*, vol. 62, no. 5, pp. 2822–2826, May 2014.
[16] Q. Liu, J. Shen, J. Yin, H. Liu, and Y. Liu, "Compact 0.92/2.45-GHz dual-band directional circularly polarized microstrip antenna for handheld RFID reader applications," *IEEE Trans. Antennas Propag.*, vol. 63, no. 9, pp. 3849–3856, Sep. 2015.
[17] J. Zhang and Z. Shen, "Dual-band shared-aperture UHF/UWB RFID reader antenna of circular polarization," *IEEE Trans. Antennas Propag.*, vol. 66, no. 8, pp. 3886–3893, Aug. 2018.
[18] C. C. Cruz, J. R. Costa, and C. A. Fernandes, "Hybrid UHF/UWB antenna for passive indoor identification and localization systems," *IEEE Trans. Antennas Propag.*, vol. 61, no. 1, pp. 354–361, Jan. 2013.
[19] M. Fantuzzi, D. Masotti, and A. Costanzo, "A novel integrated UWB-UHF one-port antenna for localization and energy harvesting," *IEEE Trans. Antennas Propag.*, vol. 63, no. 9, pp. 3839–3848, Sep. 2015.
[20] D. L. Nguyen, K. S. Paulson, and N. G. Riley, "Reduced-size circularly polarized square microstrip antenna for 2.45 GHz RFID applications," *IET Microw., Antennas Propag.*, vol. 6, no. 1, pp. 94–99, Aug. 2011.
[21] M. Lalkota, G. Gupta, V. K. Pandit, and A. R. Harish, "UHF reader antennas system for near and far-field RFID operation," *IEEE J. Radio Freq. Identif.*, vol. 3, no. 1, pp. 14–24, Mar. 2019.
[22] M. Alibakhshi-Kenari, M. Naser-Moghadasi, R. A. Sadeghzadeh, B. S. Virdee, and E. Limiti, "Dual-band RFID tag antenna based on the Hilbert-curve fractal for HF and UHF applications," *IET Microw., Antennas Propag.*, vol. 10, no. 2, pp. 140–146, Aug. 2015.
[23] K. R. Jha, B. Bukhari, C. Singh, G. Mishra, and S. K. Sharma, "Compact planar multistandard MIMO antenna for IoT applications," *IEEE Trans. Antennas Propag.*, vol. 66, no. 7, pp. 3327–3336, Jul. 2018.

[24] G. Shi, Y. He, B. Yin, L. Zuo, P. She, W. Zeng, and F. Ali, "Analysis of mutual couple effect of UHF RFID antenna for the Internet of Things environment," *IEEE Access*, vol. 7, pp. 81451–81465, 2019.
[25] A. D. Serio, J. Buckley, J. Barton, R. Newberry, M. Rodencal, G. Dunlop, and B. O'Flynn, "Potential of sub-GHz wireless for future IoT wearables and design of compact 915 MHz antenna," *Sensors*, vol. 18, no. 22, pp. 2–25, 2018.
[26] (2017). *NXP Semiconductor PN532/C1 Near Field Communication (NFC) Controller Product Datasheet*. Accessed: Nov. 28, 2017. [Online]. Available: https://www.nxp.com/docs/en/nxp/data-sheets/PN532_C1.pdf
[27] (2012). *AMS AS3993 UHF RFID Reader Product Datasheet*. Accessed: Jun. 26, 2012. [Online]. Available: https://www.ams.com
[28] CST. (2006). *CST Microwave Studio Suite User's Manual*. Accessed: Sep. 14, 2006. [Online]. Available: https://www.cst.com
[29] M. Alibakhshi-Kenari, M. Naser-Moghadasi, R. A. Sadeghzadeh, B. S. Virdee, and E. Limiti, "New compact antenna based on simplified CRLH-TL for UWB wireless communication systems," *Int. J. RF Microw. Comput. Aided Eng.*, vol. 26, no. 3, pp. 217–225, Mar. 2016.
[30] R. A. Sadeghzadeh, M. Alibakhshi-Kenari, and M. Naser-Moghadasi, "UWB antenna based on SCRLH-TLS for portable wireless devices," *Microw. Opt. Technol. Lett.*, vol. 58, no. 1, pp. 69–71, Jan. 2016.
[31] M. Alibakhshi-Kenari, A. Andújar, and J. Anguera, "New compact printed leaky-wave antenna with beam steering," *Microw. Opt. Technol. Lett.*, vol. 58, no. 1, pp. 215–217, 2016.
[32] M. Alibakhshi-Kenari, M. Naser-Moghadasi, R. A. Sadeghzadeh, and B. S. Virdee, "Hexa-band planar antenna with asymmetric fork-shaped radiators for multiband and broadband communication applications," *IET Microw., Antennas Propag.*, vol. 10, no. 5, pp. 471–478, Apr. 2016.
[33] M. Alibakhshi-Kenari, M. Khalily, B. S. Virdee, C. H. See, R. A. Abd-Alhameed, and E. Limiti, "Mutual-coupling isolation using embedded metamaterial EM bandgap decoupling slab for densely packed array antennas," *IEEE Access*, vol. 7, pp. 5182–51840, 2019.
[34] M. Alibakhshi-Kenari, M. Naser-Moghadasi, R. A. Sadeghzadeh, B. S. Virdee, and E. Limiti, "Periodic array of complementary artificial magnetic conductor metamaterials-based multiband antennas for broadband wireless transceiver," *IET Microw., Antennas Propag.*, vol. 10, no. 15, pp. 1682–1691, Dec. 2016.
[35] M. Alibakhshi-Kenari, M. Naser-Moghadasi, R. A. Sadeghzadeh, B. S. Virdee, and E. Limiti, "Traveling-wave antenna based on metamaterial transmission line structure for use in multiple wireless communication applications," *AUE-Int. J. Electron. Commun.*, vol. 70, no. 12, pp. 1645–1650, Dec. 2016.
[36] M. Alibakhshikenari, B. S. Virdee, M. Khalily, P. Shukla, C. H. See, R. A. Abd-Alhameed, F. Falcone, and E. Limiti, "Beam-scanning leaky-wave antenna based on CRLH-metamaterial for millimeter-wave applications," *IET Microw., Antennas Propag.* vol. 13, no. 8, pp. 1129–1133, Jul. 2019.
[37] M. Alibakhshi-Kenari, M. Khalily, B. S. Virdee, C. H. See, R. A. Abd-Alhameed, and E. Limiti, "Mutual-couling suppression between two closely placed microstrip patches using EM-bandgap metamaterial fractal loading," *IEEE Access*, vol. 7, pp. 23606–23614, 2019.
[38] M. Alibakhshi-Kenari, M. Naser-Moghadasi, R. A. Sadeghzadeh, and B. S. Virdee, "Metamaterial-based antennas for integration in UWB transceivers and portable microwave handsets," *Int. J. RF Microw. Comput. Aided Eng.*, vol. 26, no. 1, pp. 88–96, Mar. 2016.
[39] M. Alibakhshi-Kenari, M. Naser-Moghadasi, R. A. Sadeghzadeh, B. S. Virdee, and E. Limiti, "A new planar broadband antenna based on meandered line loops for portable wireless communication devices," *Radio Sci.*, vol. 51, no. 7, pp. 1109–1117, Jul. 2016.
[40] M. Alibakhshi-Kenari, M. Naser-Moghadasi, R. A. Sadeghzadeh, B. S. Virdee, and E. Limiti, "Bandwidth extension of planar antennas using embedded slits for reliable multiband RF communications," *AEU-Int. J. Electron. Commun.*, vol. 70, no. 7, pp. 910–919, Jul. 2016.

ADISAK ROMPUTTAL received the B.Eng. and M.Eng. degrees in electronics engineering, and the D.Eng. degree in electrical engineering from the King Mongkut's Institute of Technology Ladkrabang (KMITL), Thailand, in 2002, 2004, and 2017, respectively. He is currently an Assistant Professor with the Department of Physics, Faculty of Science and Technology, Thammasat University, Thailand.

CHUWONG PHONGCHAROENPANICH received the B.Eng. (Hons), M.Eng., and D.Eng. degrees from the King Mongkut's Institute of Technology Ladkrabang (KMITL), Bangkok, Thailand, in 1996, 1998, and 2001, respectively. He is currently an Associate Professor with the Department of Telecommunications Engineering, KMITL, where he also serves as the Leader of the Innovative Antenna and Electromagnetic Applications Research Laboratory. His research interests include antenna design for various mobile and wireless communications, conformal antennas and array antenna theory. He is a member of IEICE and ECTI. He was the Chair of the IEEE MTT/AP/ED Thailand chapter. He has been the organizing committee of several international conferences including the TPC Chair of 2009 International Symposium on Antennas and Propagation (ISAP2009) and TPC member of ISAP2012. He is currently an Editorial Board of the *International Journal of RF and Microwave Computer-Aided Engineering* and an Associate Editor for IEICE ComEx. He was an Associate Editor for *IEICE Transactions on Communications*, and *ECTI Transactions on Electrical Engineering, Electronics, and Communications*. He is the Reviewer of many scientific journals including the IEEE TRANSACTIONS ON ANTENNAS AND PROPAGATION, IEEE ACCESS, *IET Microwaves, Antennas and Propagation*, *Electronics Letters*, *ECTI Transactions* and many international conferences including ISAP and APMC. He was with the Board Committee of the ECTI Association from 2008 to 2011 and from 2014 to 2015.